Ultrasound-Triggered Controlled Drug Delivery and Biosensing Using Silica Nanotubes

ARTICLE *in* THE JOURNAL OF PHYSICAL CHEMISTRY C · APRIL 2009

Impact Factor: 4.77 · DOI: 10.1021/jp9000863 · Source: OAI

2 AUTHORS:

Shobhna Kapoor
Max Planck Institute of Molecular Physiology
25 PUBLICATIONS **338** CITATIONS

SEE PROFILE

Aninda J. Bhattacharyya
Indian Institute of Science
84 PUBLICATIONS **1,377** CITATIONS

SEE PROFILE

Article

Ultrasound-Triggered Controlled Drug Delivery and Biosensing Using Silica Nanotubes

Shobhna Kapoor, and Aninda J. Bhattacharyya

J. Phys. Chem. C, **2009**, 113 (17), 7155-7163• DOI: 10.1021/jp9000863 • Publication Date (Web): 02 April 2009

Ultrasound-Triggered Controlled Drug Delivery and Biosensing Using Silica Nanotubes

Shobhna Kapoor and Aninda J. Bhattacharyya*

Solid State and Structural Chemistry Unit, Indian Institute of Science, Bangalore 560012, India

Received: January 05, 2009; Revised Manuscript Received: March 09, 2009

Silica nanotubes (SNTs) have been demonstrated here as a versatile host for controlled drug delivery and biosensing. The sol−gel template synthesized SNTs have a slow rate of drug release. Application of an external stimulus in the form of ultrasound to or chemical functionalization of synthesized SNT results in higher yield of drug release as well as yield of drug release varying linearly with time. In case of controlled drug delivery triggered by ultrasound, drug yield as function of time is found to be heavily dependent on the ultrasound impulse protocol. Impulses of shorter duration (∼0.5 min) and shorter time intervals between successive impulses resulted in higher drug yields. Confinement of hemoglobin (Hb) inside nanometer sized channels of SNT does not have any detrimental effect on the native protein structure and function. Observance of significant enhancement in direct electron transfer of Hb makes the SNTs also promising for application in biosensors.

1. Introduction

Nanostructured materials[1] have found widespread applications in diverse fields ranging from catalysis[2] to energy storage[3] to biotechnology.[4−10] The versatile nature of these materials is attributed to various factors. The presence of a large parameter basis set allows development of materials in various spatial dimensions with optimized architectures tailored for specific functions. Inorganic nanostructured materials have gained considerable importance in several biotechnological applications related to drug delivery, composite materials for implants, and sensing. Inorganic materials exhibit more superior structural and chemical stability compared to organic materials. While biocompatibility may not be a serious issue, a high degree of (chemical) stability may pose problems for generating biodegradable inorganic systems under physiological conditions. In this regard, soft-matter organic systems such as polymers [11,12] have been the natural choice for several biotechnological applications such as drug delivery. The polymeric systems offer several avenues for chemical manipulation to make them biocompatible as well as biodegradable in aqueous medium. However, the success rate for real applications has been low because the process of controlled biodegradation, in general, is a nontrivial problem and usually correlated to several other physiological issues such as toxicity. So, inspite of being in the early stages from the point of view of applications, the inorganic nanostructured systems offer an attractive alternative and may even serve as model systems for improvement of prevailing organic systems and development of new systems such as organic−inorganic hybrids.[5]

Inorganic porous materials have attracted considerable attention as hosts for immobilization of a variety of guest molecules [6−10,13,14] such as proteins, drugs, and smaller biological molecules (amino acids, peptides, vitamins). Mesoporous oxides such as e.g. MCM-type silica and SBA-type silica have already been demonstrated as a promising host for drug delivery.[10,13,14] It has been shown rather convincingly that both degree of drug loading and rate of release heavily depend on several oxide substrate parameters such as pore size, pore surface area, and surface chemical moieties. These parameters are crucial as they decide the ability of the substrate to deliver drug and sustain concentrations within the therapeutic window.[12] It has also been demonstrated that confinement of the biomolecules of varying sizes inside the empty space formed by pore arrays [7−9] do not seem to have any adverse affect on the molecular structure and function. In certain cases molecular activity has been enhanced in confinement compared to that in the free state. Apart from mesoporous systems, other nanostructured materials such as nanotubes have also been employed for drug delivery as well as for nanoconfinement of macromolecules.[8,9] Immobilization of various types of proteins inside carbon nanotubes resulted in an enhancement of electroactivity of the protein. Further, composites of carbon nanotubes with various proteins, such as enzymes, have been demonstrated as potential electrode systems in biosensors. In the present work we demonstrate silica nanotubes synthesized by a sol−gel template method[15] as potential hosts for controlled drug delivery. Suitable chemical functionalization or external stimulation via ultrasound of the synthesized SNT resulted in controlled drug delivery of ibuprofen (IBU). We also show that the same silica nanotube can also be effectively employed to confine a heme protein such as hemoglobin, and the SNT-protein composite system can be used as an electrode in a biosensor.

2. Experimental Section: Materials and Methods

Preparation of Silica Nanotubes (SNT). Silica nanotubes were prepared by the procedure described in ref 15. Commercially available Anodisc alumina membranes (Whatman Anodisc, pore diameter of 250 ± 50 nm) were immersed for 2−3 min in a solution of 10 mol % silicon tetrachloride ($SiCl_4$, Sigma) in carbon tetrachloride (CCl_4, Merck). Following immersion, the membranes were first quickly washed with CCl_4 for removal of remnant reagent from the faces and were again placed in a fresh portion of CCl_4 for 30 min to remove unbound $SiCl_4$ from the pores. After the washing procedure, the membranes were soaked in a mixture of CCl_4 and methanol (1:1 v/v) for 2 min and then in ethanol for 5 min to displace CCl_4; finally they were dried under argon atmosphere. The dried membranes were immersed in deionized water for 5 min, washed with methanol for 2 min, and then redried under argon stream.

* Corresponding author. E-mail: aninda_jb@sscu.iisc.ernet.in. Telephone: +91 8022932616. Fax: +91 8023601310.

10.1021/jp9000863 CCC: $40.75
Published on Web 04/02/2009

After this, the membranes were dissolved by keeping them immersed overnight in 70% H_2SO_4 aqueous solution at 70 °C. The sonication time was optimized for minimum damage to the nanotubes. For further centrifugation, Millipore water was added to the white sediment, and the process was repeated at least 9−10 times for complete elimination of the acid. Additionally, the decanted liquid was also centrifuged each time to ensure extraction of all nanomaterials. The sediment from the centrifugation process was dried in an air oven at 55−70 °C. The yield of silica nanotubes per synthesis using 10 Anodiscs at a time was approximately 50 mg (per Anodisc the yield varied from 5−6 mg).

Preparation of 2,3 Dihydroxynaphthalene (DN)-Coated SNT. DN-coated SNT (abbreviated hereafter as SNT-DN) were prepared according to the procedure in ref 16: 460 mg of the commercially available DN (Spectrochem) was dissolved in 2 mL of acetone, followed by the addition of 94 mg of SNT while stirring the solution. The solution was aged overnight while stirring. After evaporation of acetone at 95 °C the resulting solid mixture of DN and SNT was heated under N_2 flow at 300 °C[17] for 1 h. At this step, dehydration occurs by the reaction between the silanol groups and the hydroxyl groups of the DN.[18] The unreacted DN was removed by centrifuging the solution with acetone for 1 min. Finally, the mixture was dried to remove acetone.

Ibuprofen (IBU) Purification. Commercially available ibuprofen (IBU) was purified prior to the preparation of the composites. For the purification, IBU was first dissolved in ethanol (at 50 °C) and stirred for a while in a beaker. The beaker containing the IBU−ethanol mixture was cooled immediately to approximately 10 °C and kept at that temperature overnight. After being defrosted at room temperature, the solution was covered with a perforated lid for slow evaporation under laboratory air. Pure dry crystals were obtained after approximately 4−5 days of drying.

Impregnation of SNT and SNT-DN with IBU. The requisite amount of pure IBU was added to hexane to yield a solution with drug (in milligrams) to solvent (in milliliters) ratio, $a_{IBU} = 20$ mg/mL. The SNT and SNT-DN were immersed in the drug solution overnight at 4 °C followed by drying at 55 °C overnight. SNT and SNT-DN impregnated with IBU are designated as SNT:IBU and SNT-DN:IBU, respectively.

Impregnation of SNT with Hb. Hemoglobin [Hb (human Hb, MW 65000] in the amount of 2.5 mg was mixed with 10 mg/mL solution of SNT in 0.1 M PBS (pH 7.0) and kept at 4 °C. SNT impregnated with Hb is designated as SNT:Hb.

Characterization Techniques for Probing of Drug Loading in SNT/SNT-DN and Hemoglobin (Hb) in SNT. The extent of IBU loading in SNT/SNT-DN and Hb in SNT was studied using thermogravimetry analysis (TGA), X-ray diffraction (XRD), and Fourier transform infrared (FTIR) spectroscopy. The TGA (Perkin-Elmer Pyris6000) experiments were done by heating the sample in a silica crucible under nitrogen atmosphere from room temperature (= 25 °C) to 750 °C at a heating rate of 10 °C/min. Wide angle XRD (Phillips X'Pert Pro-diffractometer, Cu Kα radiation, $\lambda = 1.5418$ Å) data at 25 °C over the range $5° \leq 2\theta \leq 40°$ with a step width and a scan rate of 0.02° and 0.6° per minute, respectively, was collected using a multipurpose sample holder. For room temperature FTIR (Perkin-Elmer FTIR Spectrometer Spectrum 1000) measurements, requisite amounts of SNT/SNT:IBU/SNT-DN:IBU/SNT:Hb were mixed with pure spectroscopic grade potassium bromide (KBr) and were each cast into a pellet of diameter 1.3 cm and thickness ~0.1 cm. Transmission electron microscope (TEM) images were observed and recorded on a FEI Tecnai F30 with an acceleration voltage of 200 kV. Each sample was well ground with an agate pestle and mortar, dispersed in ethanol by ultrasonication, and then dropped on a Cu grid with a carbon-reinforced plastic film. Scanning electron microscopy was done using FEI SIRION in the voltage range 5−10 kV.

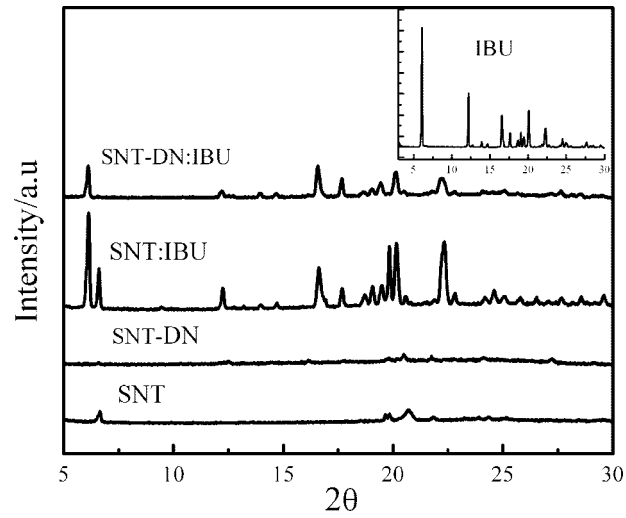

Figure 1. X-ray diffraction (XRD) patterns at 25 °C for SNT, SNT-DN, SNT:IBU, and SNT-DN:IBU. (Inset) XRD pattern of unloaded IBU.

In Vitro Drug Release Kinetics. Release of IBU from SNT:IBU and SNT-DN:IBU was studied in simulated body fluid (SBF). The concentration of SNT:IBU in SBF was 3 mg/mL. SBF of pH = 7.2 was prepared as per the prescription in ref 19 The SBF composition is as follows: 0.14 M (Na^+), 0.005 M (K^+), 0.0025 M (Ca^{2+}), 0.0015 (Mg^{2+}), 0.15 M (Cl^-), 0.0042 M (HCO_3^-), 0.001 M (HPO_4^{2-}), 0.0005 M (SO_4^{2-}). IBU release kinetics was observed by monitoring the characteristic peak at 264 nm of IBU by UV−vis spectroscopy (Perkin-Elmer, Lambda 35 UV spectrometer). Ultrasound impulses (33 ± 2 kHz) of duration ranging from 0.5 min to continuous and with rest times between successive impulses ranging from 0 to 30 min were given to the SNT-IBU composite during release kinetics. IBU release kinetics under ultrasound impulse was done at 25 °C (±1 °C).

Preparation of Modified Working Electrode for Biosensing. Prior to modification the glassy carbon electrode (GCE, 3 mm diameter) was rinsed with water and ultrasonicated in water bath. Ten microliters of SNT:Hb and Hb was dropped on the shining surface of GCE and dried for 3−4 h at room temperature. The modified electrodes were referred to as SNT/Hb/GCE and Hb/GCE.

Cyclic Voltammetry for Measuring Electroactivity of Hemoglobin (Hb). For cyclic voltammetry measurements (CHI 608C), the working electrode was either SNT/Hb/GCE or Hb/GCE electrode. Saturated calomel electrode was used as the reference electrode, and a Pt wire served as the counter electrode. The working solution (5 mL of 0.1 M PBS, pH 7.0) was deoxygenated for 30 min prior to start of the measurement, and nitrogen atmosphere was maintained throughout the experiment.

3. Results and Discussion

Evidence for Impregnation of SNT and SNT-DN with IBU and SNT with Hb. ***X-ray Diffraction (XRD) Studies.*** Figure 1 shows the XRD patterns for the SNT/SNT-DN bare and loaded

with IBU. Except for the observance of peaks at $2\theta = 6.6°$ and 22° for SNT, the XRD patterns of the bare SNT and SNT-DN are predominantly amorphous in nature.[20] For SNT loaded with IBU, peaks at $2\theta = 6.1°$, 12.2°, 16.5°, 17.2°, 18.6°, 19.0°, 19.4°, 20.1°, 22.3°, 22.7°, and 24.6° are attributed to those of pure IBU (inset of Figure 1). The IBU peaks were less intense and broader compared to those observed for free IBU. This is attributed to the interaction of IBU with OH groups on SNT which results in a certain degree of disorder and smaller crystallites compared to free IBU. This is evident from the change in crystallite size obtained from XRD using the Scherrer formula. The IBU crystallite size considering the peak at $2\theta = 6.1°$ changed from 1.5 nm for free IBU to 1.4 nm for SNT:IBU and 1.3 nm for SNT-DN:IBU. As will be discussed later, the synthesized SNTs show a higher IBU loading compared to that in SNT-DN. The higher IBU loading is probably the reason for the appearance of sharper peaks in the case of SNTs compared to that in SNT-DN (the intensities in both cases being lesser than that for free IBU). Sharper diffraction peaks in the case of SNT:IBU is also attributed to probable residence of some fraction of IBU on the outer surface of SNT.

Fourier-Transform Infrared (FTIR) Studies. Panels a and b of Figure 2 show the Fourier transform infrared (FTIR) spectra of SNT, SNT-DN, SNT:IBU, SNT-DN:IBU and IBU. The observed band between 3700−3500 cm^{-1} for SNT is attributed to Si−OH stretching frequency.[21,22] The OH stretch band almost diminishes upon functionalization with DN, suggesting that all silanol groups on the SNT have reacted with DN. Surface functionalization with DN also results in the appearance of several new peaks. Bands at 1500 cm^{-1} and 750 cm^{-1} are attributed to C=C stretching vibrations and out-of-plane deformation, respectively.[21] Furthermore, the stretching frequencies observed at 1050−1100 cm^{-1} and 1618−1660 cm^{-1} are respectively due to Si−O−Si stretching and frame symmetric and asymmetric flexible vibrations of Si groups.[23] Reduction in the *C*=OOH band intensity at approximately 1718 cm^{-1} was observed more for SNT:IBU than for SNT-DN:IBU. This suggests the existence of a stronger interaction between IBU and OH groups on SNT. Evidence in support of the IBU-SNT interaction can also be observed from the appearance of a less intense $C{=}OO^-$ asymmetric stretch band at approximately 1600 cm^{-1}. No such band was observed in the case of the SNT-DN: IBU sample, suggesting a much weaker interaction due to hydrophobic DN coverage of SNT. Signs of IBU disorder (observed in XRD) after adsorption on SNT is also observed in FTIR via decrease in intensity at 1417 cm^{-1} (C−O−H in plane bending band) and 939 cm^{-1} disappearance of O−H (out-of-plane bending band). Figure 2c shows the FITR results for impregnation of SNT with Hb. The spectrum of Hb shows the following signature bands: amide I around 1650 cm^{-1} due to C=O stretching vibration of peptide linkages in the protein backbone and amide II band around 1550 cm^{-1} which results from a combination of N−H bending and C−N stretching. These bands provide information on the secondary structure of the polypeptide. For SNT:Hb, the amide I and amide II bands have nearly the same contour, suggesting that Hb immobilization inside SNT did not result in any adverse effects on the native protein structure. The complete disappearance of the band at 803 cm^{-1} might result from the interaction between Hb and SNT. The observance of Soret band (from UV−vis spectroscopy) corresponding to Hb provides additional support for the absence of any structural distortion such as denaturation arising from confinement of Hb inside SNT.

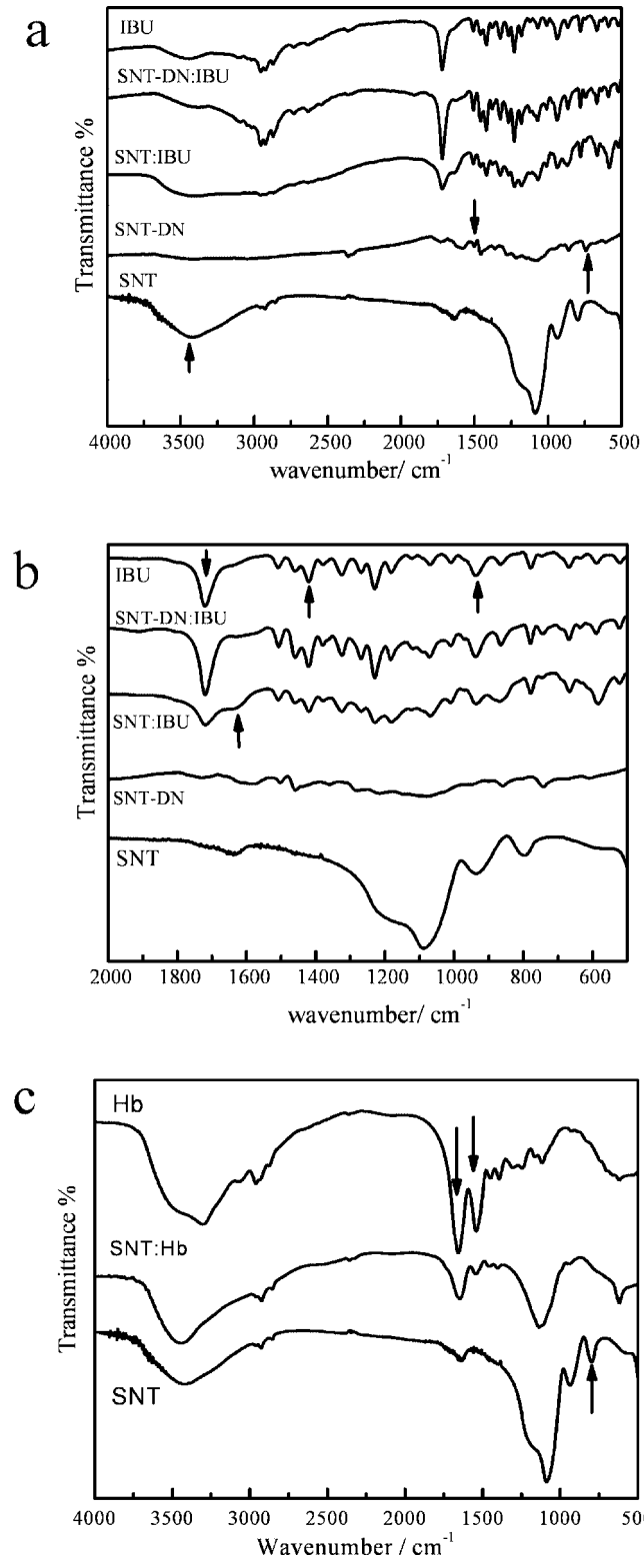

Figure 2. (a and b) FTIR at 25 °C for various samples: SNT, SNT-DN, SNT:IBU, SNT-DN:IBU, and IBU. (c) FTIR at 25 °C for SNT, SNT:Hb, and Hb.

Thermogravimetric Analysis (TGA) Studies. As described earlier, IBU was loaded into SNT by immersing the nanotubes in hexane solution of ibuprofen. Despite certain adverse effects, hexane has been the solvent of choice for several research groups including the group of Regí-Vallet who have done pioneering work related to application of mesoporous silica materials as drug delivery systems[10] and also based on our prior experience

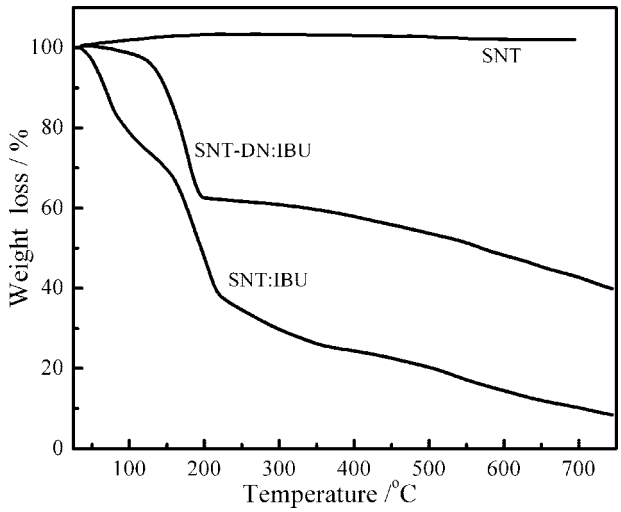

Figure 3. Thermogravimetry analysis (TGA) of various samples (temperature range: 25−750 °C, heating rate: 10 °C/min): SNT, SNT-DN:IBU, and SNT:IBU.

with respect to mesoporous alumina.[14] One reason for the frequent usage is the high degree of IBU solubility in hexane (40 mg/mL) compared to that in other nonaqueous solvents, which in general results in a higher drug loading in nanostructured porous materials such as mesoporous matrices and nanotubes.[10,24] The other important advantage is that hexane, being highly volatile, evaporates rapidly out of the composite mixture, which in turn leads to shorter sample preparation times. Figure 3 shows thermogravimetry analysis results of bare and IBU loaded SNT. For the bare SNT no significant weight loss was observed in the temperature range 40−750 °C. For SNT:IBU, weight loss of 46% (estimated assuming 190 °C as the initial temperature) is attributed essentially to IBU. In the case of SNT-DN:IBU the estimated weight loss due to IBU was approximately 25% (loss due to DN: 5−10%).

Transmission Electron Microscopy (TEM). Figure 4 shows both the transmission (a−c, f−j) and scanning electron micrographs (d, e) of bare nanotubes and nanotubes impregnated with IBU and Hb. The morphologies of the bare nanotubes are shown in Figure 4a−c, f. Bare nanotubes are arranged in bundles (scanning electron micrograph, Figure 4e) with an average length of 10 μm, inner and outer diameters being approximately 200 and 300 nm, respectively. (As the SNT yield per synthesis was low, it was not possible to carry out detailed nitrogen adsorption/desorption experiments for estimation of pore volume in the various SNT. Some preliminary nitrogen adsorption/desorption measurements were performed with bare SNT and SNT-DN. The pore volumes for bare SNTs were estimated to be approximately 0.24 $cm^3\ g^{-1}$ and for SNT-DN were 0.07 $cm^3\ g^{-1}$). The nanotubes do not have uniform diameter throughout the entire length and are usually open on one end (Figure 4d). The other ends of the tube in a majority of cases were found to be closed (Figure 4c) in a rounded manner similar to that of a round-bottom glass tube (Figure 4c). The tubes are also marked by junctions such as y-junctions (Figure 4b) and bends (from SEM as in Figure 4d). We attribute the heterogeneities in nanotube morphology to the starting alumina membranes. The membranes (Supporting Information, Figure 1) have considerable dispersion in both diameter of pore as well as the columnar channel (250 ± 50 nm). As discussed later, the structural heterogeneities of the nanotubes play a key role in the release kinetics of the drug. Figure 4g shows TEM for bare SNT-DN. DN coverage of SNT results in an increment of the outer diameter from 300 nm to approximately 350 nm. The high degree of impregnation of SNT with IBU and Hb is also demonstrated via TEM (Figure 4h−j). TEM also shows a small fraction of IBU residing outside SNT (Figure 4j) and SNT-DN nanotubes (not shown here).

In Vitro Release Kinetics of Ibuprofen from SNT. Figure 5 shows the in vitro release profile at 25 °C of ibuprofen from SNT into the simulated body fluid (SBF) (3 mg/mL) at 25 °C. The release kinetics of IBU from SNT is slow. Only ∼20% of IBU is released into SBF after monitoring for nearly 30 h. We attribute the slow release to the various heterogeneities present in the SNT. The nonuniformity in tube diameter and the presence of junctions and bends pose steric hindrance for fast diffusion of solvent molecules into and counter diffusion of the solvated drug out of the nanotube. This results in slow IBU release from SNT. In comparison, pure MCM-type materials such as MCM-48 (synthesized as per ref 10 average pore size: 2.5 nm, BET surface area = 1241 $m^2\ g^{-1}$; pore volume ∼1 $cm^3\ g^{-1}$) show approximately 90% release within 30 h. The efficiency of a drug-carrying host releasing drug in a controlled manner is determined by the residence time of drug concentrations within the therapeutic window[12] for the particular drug. In the present study considering the drug release yields over a period of 24 h (Figure 5) MCM-48 results in a higher dosage of 0.075 mg/kg·bw/day (bw: body weight, bw = 60 kg), whereas SNT would result in a lower dosage 0.02 mg/kg·bw/day (bw = 60 kg). The IBU kinetics change significantly as a result of functionalization of SNT surface with the model chemical moiety, 2,3-dihydroxynaphthalene (DN). On the whole, the IBU release kinetics from SNT-DN is intermediate to that of SNT and MCM-48. After approximately 13 h the IBU release yield in SBF from SNT-DN becomes higher than that for MCM-48. Nearly about 95% of IBU is released in 24 h compared to 87% for MCM-48 and 20% for SNT. This implies an estimated dosage of 0.04 mg/kg·bw/day (bw = 60 kg) for SNT-DN:IBU. As no numerical estimates for IBU dosages using controlled drug delivery systems are available, it is not possible to judge at this juncture the extent of clinical utility of the SNT or SNT-DN controlled drug delivery systems. However, the dosages obtained for SNT and SNT-DN were found to be much lower in comparison to the maximum recommended therapeutic dosages (MRTD) for oral delivery (∼40 mg/kg·bw/day, [25]). We believe that the drug dosages obtained for SNT and SNT-DN can be further tuned via optimization of morphological parameters of the nanotubes. Compared to MCM-48 which shows drug release of close to 60% in the first 3 h, less than 22% IBU is released from SNT-DN. In addition to the steric hindrances, the slow release in the case of SNT-DN is attributed to the dominance of attractive interaction (such as $\pi-\pi$) between the surface naphthalene group and IBU over that of solvation of IBU (i.e., the COOH group) by the SBF. Significant amount of IBU release takes place only when a sufficient amount of solvent molecules has diffused through the channels of the nanotubes for solvation of the drug. (Existence of diffusion[26] is supported via existence of a linear relationship between amount of IBU released, [IBU] versus square root of time, $[IBU] = 19.5t^{0.5}$, over 16 h for SNT-DN.) The faster release of IBU at longer time scales from SNT-DN compared to that from MCM-48 (average pore size ∼2.5 nm) is attributed to the difference in morphology of the nanostructured materials. As the nanotube diameter is wider compared to the pores of MCM-48, one expects a faster diffusion of the solvent into tube channels as well as a faster counter diffusion of IBU out of the nanotube. We propose that surface functionalization of nanostructure-based drug delivery

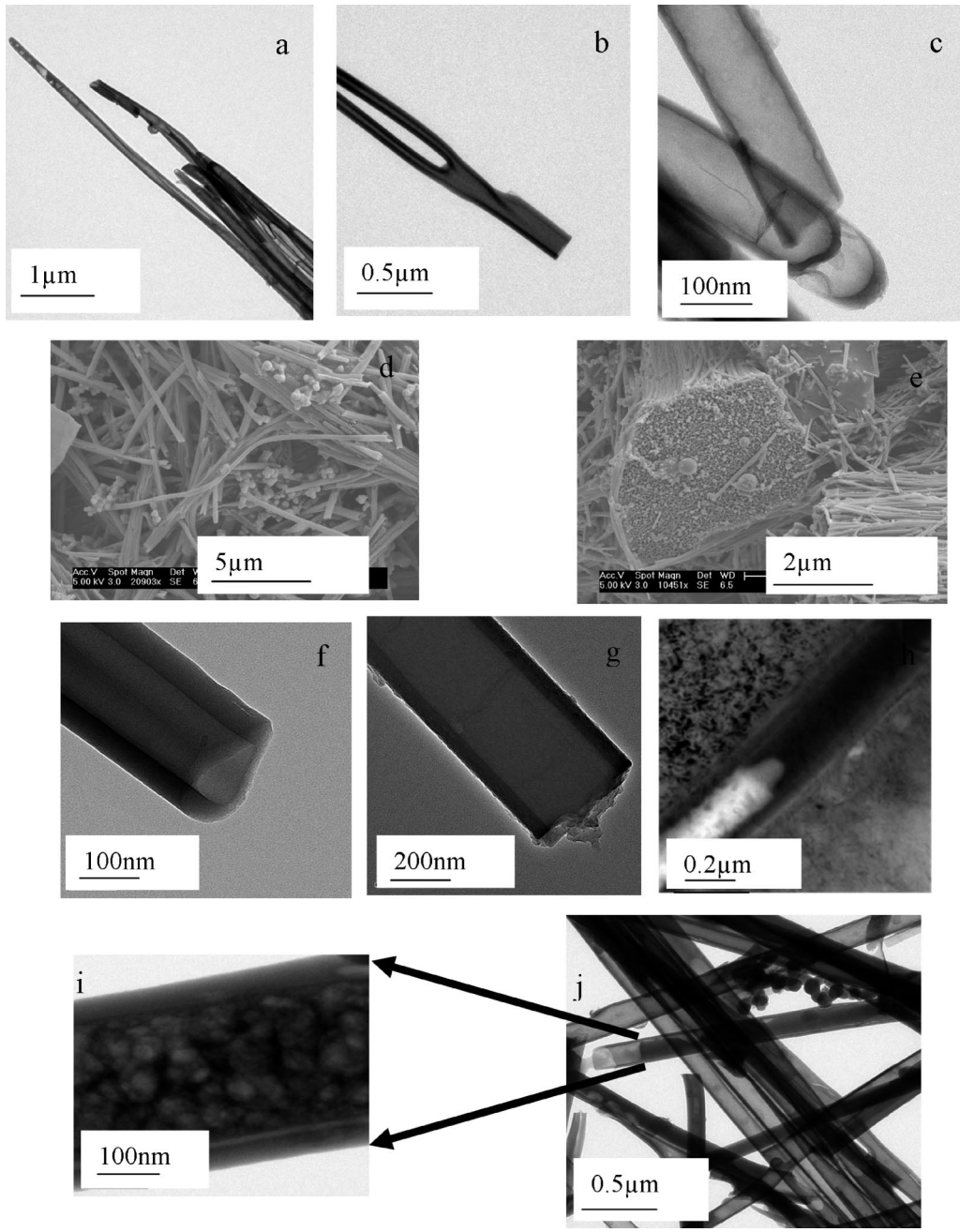

Figure 4. (a−c, f) Transmission electron microscope (TEM) images showing the general morphology of the bare SNT nanotubes before kinetics, (a) bundles of SNT nanotubes of approximately 10 μm long, (b) y-junction in SNT, (c) closed ends of SNT, (f) open ends of SNT, (g) increase in nanotube diameter of SNT due to DN coverage, (h) impregnation of SNTs with Hb, (i, j) impregnation of SNTs with IBU micrographs also show some fraction of IBU residing outside the SNT (h). Scanning electron microscope (SEM) of nanotubes of bare SNTs before kinetics (d) bends in SNTs, (e) bundles of SNT.

systems with chemical moieties having similar physicochemical properties as DN but more physiologically compatible than DN will be highly beneficial for controlled drug release. DN or in general chemical groups such as DN which are partially or sparingly soluble in aqueous solution allow retention of drug concentrations within the therapeutic window for longer periods of time and also aid in targeted release.

We now demonstrate an alternative procedure for controlled release of IBU from synthesized SNT using ultrasound as an external stimulus. Ultrasound-triggered drug release on mesoporous silica has already been reported. In ref 27 drug release from MCM-41/-48 matrix modified with PDMS was studied under the application of ultrasound impulses. In ref 28 electrical stimuli were given to the polymer matrix composite (PEOx and PMMA) loaded with insulin, and stepwise release of insulin was observed. The purpose of application of an external stimulus will be highly beneficial for the solvent molecules as well as solvated drug to overcome several nanotube morphological heterogeneities (Figure 4) such as junctions, bends, and nonuniformity in thickness. Panels a−d of Figure 6 show the release profile of IBU from SNT under various ultrasound impulse protocols. For all impulse protocols, the first impulse was applied after monitoring IBU release for 1000 min (SEM shows that SNT bundles as observed in Figure 4e remain intact after the kinetics in the absence of any ultrasound impulse). Figure 7 shows SEM and TEM done after the application of ultrasound impulses. Figure 6a shows the release profile under impulses of 1 min duration given every 5 min. In a span of approximately

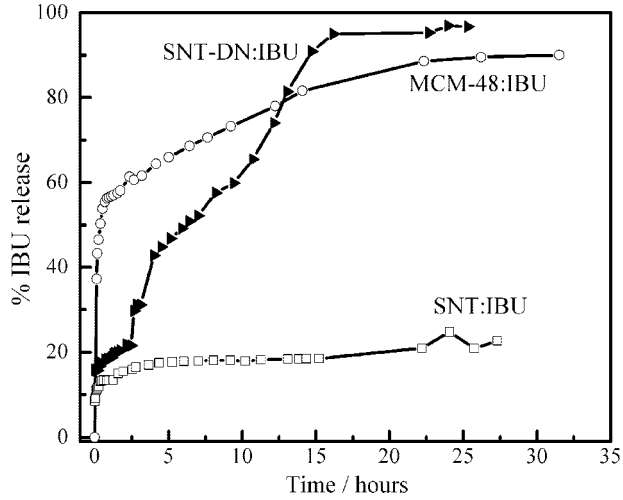

Figure 5. Kinetics of IBU release in SBF (pH = 7.3) from various samples: MCM-48:IBU, SNT:IBU, and SNT-DN:IBU (drug release kinetics observed via monitoring characteristic peak at 264 nm of IBU by UV−vis spectroscopy).

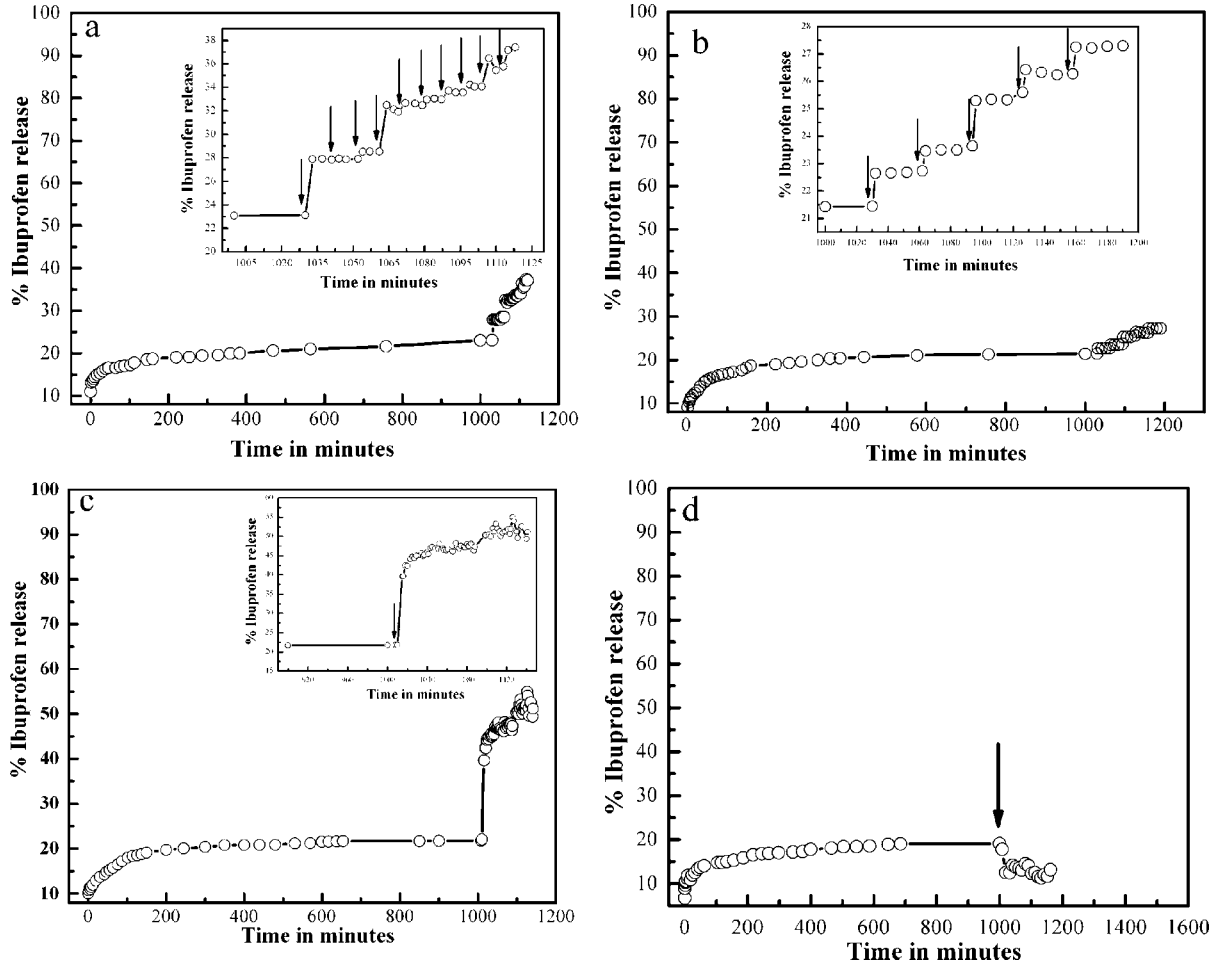

Figure 6. Kinetics of IBU release in SBF (pH = 7.3) from SNT:IBU under various ultrasound impulse protocols: (a) 1 min duration impulse with 5 min rest time; (b) 1 min duration impulse with 30 min rest time; (c) 0.5 min duration impulse with 2 min rest time; and (d) continuous impulse with no rest time (drug release kinetics observed via monitoring characteristic peak at 264 nm of IBU by UV−vis spectroscopy).

90 min (total number of impulses = 10) the yield of IBU release increased by approximately 13% from 24% to 37%. Figure 6b shows the release profile with impulses of the same duration (i.e., 1 min) but with a different interval of 30 min. A total of five impulses were given over a period of 160 min. IBU release yield increased from 22% to 28% over the time period. The higher yield of IBU in SBF under the application of ultrasound impulse is attributed to the removal of various heterogeneities of the nanotubes which otherwise pose steric hindrance to the flow of solvent molecules and the solvated drug molecule. The bundles of SNT observed prior to the application of impulses (Figure 4e) are no longer observed for the sample to which impulses of 1 min duration at 5 min intervals were applied (SEM, Figure 7a). Instead only single tubes of shorter length trapped in the debris of the tubes and drug were observed. This is also confirmed via TEM. Darker background is due to the

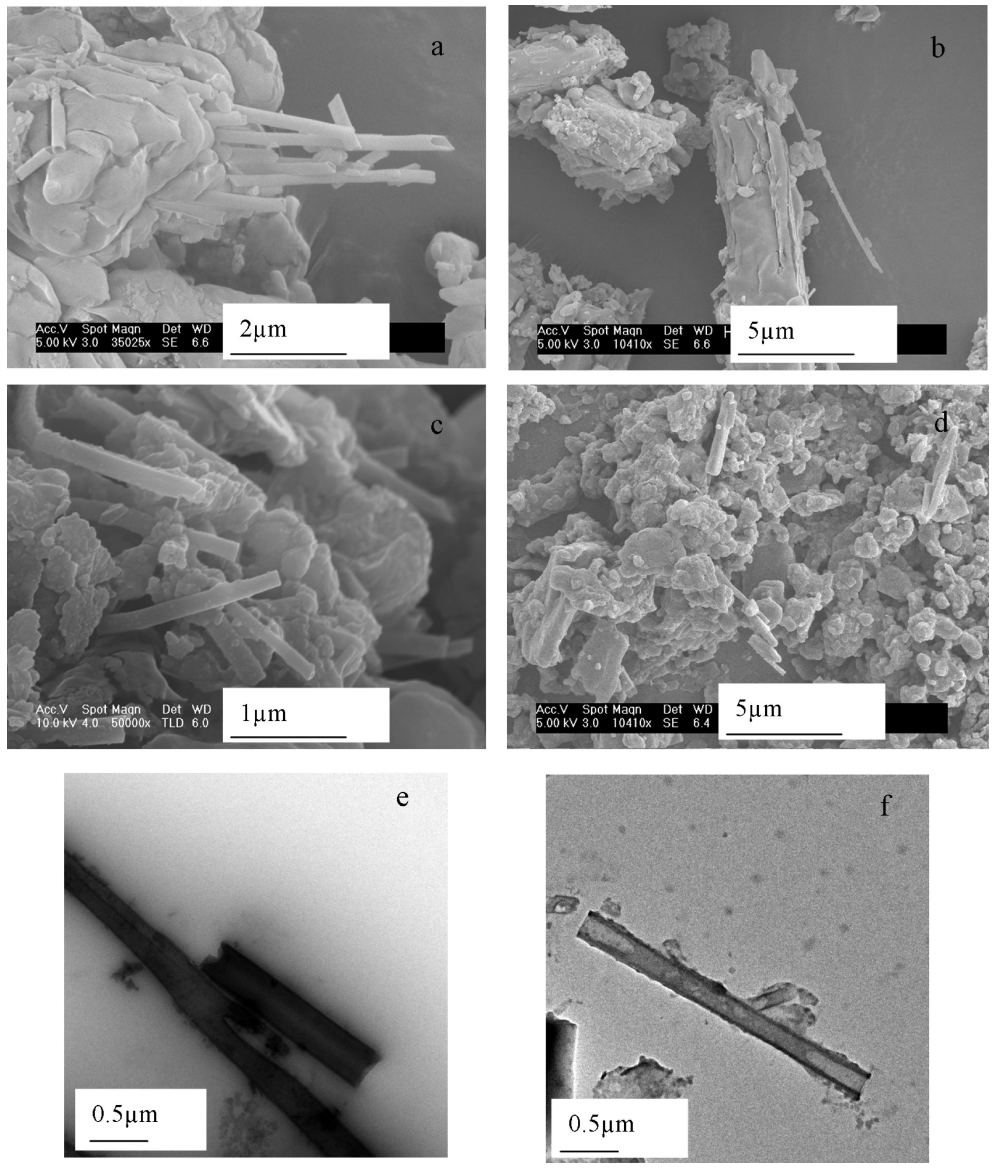

Figure 7. Scanning electron microscope images of SNT:IBU system post kinetics: (a) SNT-IBU with 1 min duration impulse with 5 min rest time; (b) SNT:IBU with 1 min duration impulse and 30 min rest time; (c) 0.5 min duration impulse with 2 min rest time; (d) SNT:IBU with continuous impulse, i.e. no rest time; (e−f) transmission electron microscope (TEM) images of SNT:IBU with 0.5 min impulse and 2 min rest time.

debris of the SNT and also due to released drug molecules. TEM shows clearly tubes of shorter length and devoid of any joints. This supports the observation of increased drug release from the nanotubes. However, increase in the rest time between impulses (keeping impulse duration constant at 1 min) from 5 to 30 min resulted in retention of longer nanotubes and SNT bundles. This supports the low percentage of drug release as all joints and closed ends which trap the IBU are probably not removed. At this juncture it appears that a larger number of impulses with shorter waiting times between impulses would result in higher drug release yields. In order to further substantiate our proposition, impulses of 0.5 min duration (rest time of 2 min; Figure 6c) and continuous impulses (i.e., no rest time between successive impulses) were applied (Figure 6d). Among the four impulse protocols, 0.5 min duration impulses resulted in the highest drug yields. An increase of almost 34% was observed over a period of 140 min. The first 0.5 min impulse resulted in an increase of 19% and with subsequent impulses the increase was approximately 0.5−1%. The increase of 19% by the first 0.5 min impulse is attributed to the formation of a favorable network of nanotube and debris (comprising essentially of broken tubes). In a short span of time the amount of debris formation is less; thus, the fraction of open ends of the tubes getting trapped in the debris will also be low. This results in large amounts of drug release from the nanotube which is observed via the large jump in the kinetic profile shown in Figure 6c. However, a greater number of impulses leads to more debris formation into which the open ends of the tubes are trapped, thereby leading to a slower release of drug from the tubes. The SEM images (Figure 7c) affirms this proposition. Lower drug yields in the case of impulses of 1 min with 5 min rest time and impulse of 1 min with 30 min rest times can also be accounted for on the basis of the formation and arrangement of debris around the nanotubes. Larger-duration impulses result in greater tube damage and hence higher debris formation. This leads to entrapment of the open ends of the tube and hence slow release of the drug. Longer rest times allow sufficient time for the debris to arrange near the nanotube open ends and hence block the exit routes for IBU from the nanotube. This explains lower release yield in case of impulse of 1 min duration with 30 min rest time compared to impulse of 1 min duration with 5 min rest time (Figure 6a, b). The adverse effect of debris

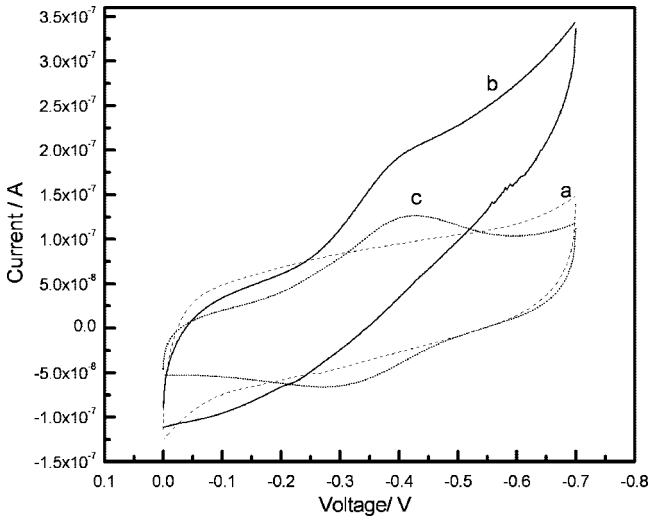

Figure 8. Cyclic voltammograms of (a) SNT/GC, (b) Hb/GC, and (c) SNT:Hb/GC in 0.1 M PBS pH 7 (scan rate: 0.01 V s^{-1}; temperature = 25 °C).

formation can be further corroborated by the results of the continuous impulse experiment as shown in Figure 6d. The release of ibuprofen from the tubes decreases after giving continuous ultrasound impulses and attains a second saturation level at around 10−12% against the one in the absence of any impulses (=20%). This is further supported by SEM (Figure 7d) which shows that applying continuous impulses leads to not only removal of heterogeneities but also results in massive destruction of SNT and creation of large amounts of debris (only a few tubes are visible Figure 7d). In the process the existing IBU outside the nanotubes in the solution gets engulfed by the tube debris, resulting in attainment of a lower saturation level. This distinctly establishes the fact that longer duration creates higher amounts of debris from the tubes into which the open end of the tubes get entrapped or the tube on the whole may get entrapped. This leads to smaller or even lower than before percent drug release. Therefore, both nanotube morphology and ultrasound protocol are key issues for optimization of drug yields under pulsatile release.

Biosensing with as Synthesized SNT. In addition to utility of SNTs as substrates for controlled drug delivery, we also demonstrate potent application of SNTs in biosensing. Several published reports have already demonstrated carbon nanotubes of various types as prospective substrates for biosensing. In the present work we show that silica nanotubes can also be used as prospective substrates for biosensing. As mentioned earlier, immobilization of Hb inside did not result in any distortion of the native structure of the protein (Figure 2c). Confinement of Hb inside SNT showed significant promotion of direct electron transfer of Hb. Figure 8 shows the cyclic voltammogram of Hb/GC, SNT/GC, and SNT-Hb/GC in 0.1 M PBS (pH 7.0). SNT/GC showed no redox peak, indicating its electro-inactivity in the measured potential range. Hb/GC showed response of Hb with only one irreversible redox peak at −0.40 V. The absence of reversible redox couple is attributed to several reasons. Strong adsorption on GC leads to reduced protein dynamics and results in a fixed number of protein configurations which may be unfavorable for the reversible electrochemical reaction. The other possibility is that adsorption on a flat surface could lead to distortion of the three-dimensional protein structure leading to denaturation which influences electroactivity. SNT:Hb/GC exhibited a pair of well-defined and reversible peaks at −0.42 and −0.31 V, corresponding to the Fe^{3+}/Fe^{2+} couple. The results demonstrate that confinement of Hb (size: 6.5 nm × 5.5 nm × 5.0 nm[29]) inside SNT has no adverse effect on the native structure as well as on the dynamics of Hb. As shown earlier (FTIR, Figure 2c), confinement results in certain degree of interaction between Hb and SNT. The SNT-IBU interaction may lead to favorable configurations resulting in better accessibility of the electroactive centers. More systematic studies such as ligand binding are needed to substantiate this point further.

Conclusions

We have demonstrated here clearly the utility of a nanostructured material such as silica nanotubes both as a controlled drug delivery system and as a biosensor. We propose systems such as SNT employed in the present study, would serve as a prototype for generation of systems having multiple functionalities for potential biotechnological applications. The parameter basis set for optimization of material properties of nanostructured systems for improved performance are diverse, ranging from dimensionality of the hosts, architecture (both internal and external), and surface chemical functionality. The host chemistry is crucial as it will determine to what extent the tailored inorganic nanostructured systems are biocompatible and biodegradable. Confinement of biomolecules such as proteins and enzymes to a region of nanometer-length scale is also interesting from a fundamental point of view. As only a few numbers of molecules, n ($1 \leq n \ll N_A$, N_A = Avogadro's number) can be accommodated in a nanostructured material such as a nanotube, we envisage that the structure−function will reflect properties of biomolecules at the mesoscopic scale. These studies will further aid in practical applications such as fabrication of miniaturized devices such as fuel cells and sensors.

Acknowledgment. We thank Indian Institute of Science (IISc.), Bangalore, for financial assistance, I.S. Jarali for BET, TGA, FTIR, A. Mondal (Institute of Nanoscience Initiative, IISc. Bangalore) for TEM.

Supporting Information Available: Scanning electron micrograph showing the starting Anodisc alumina membrane template for the synthesis of silica nanotubes. This material is available free of charge via the Internet at http://pubs.acs.org.

References and Notes

(1) (a) Vinu, A.; Miyahara, K.; Ariga, J. *Nanosci. Nanotechnol.* **2006**, *6*, 1510. (b) Rao, C. N. R.; Vivekchand, S. R. C.; Biswas, K.; Govindaraj, A. *Dalton Trans.* **2007**, *34*, 3728. (c) Vallet-Regí, M. *Dalton Trans.* **2006**, 5211. (d) Perro, A.; Reculusa, S.; Ravaine, S.; Boirgeat-Lami, E.; Duguet, E. *J. Mater. Chem.* **2005**, *15*, 3745.

(2) (a) Vinu, A.; Justus, J.; Anand, C.; Sawant, D. P.; Ariga, K.; Mori, T.; Srinivasu, P.; Balasubramanian, V. V.; Velmathi, S.; Alam, S. *Mesoporous Microporous Mater.* **2008**, *116*, 108. (b) Zhang, J.; Liu, X.; Blume, R.; Zhang, A.; Schlögl, R.; Dang, S. S. *Science.* **2008**, *322*, 73. (c) Liu, Y.; Chen, J.; Zhang, W.; Ma, Z.; Swiegers, G. F.; Too, C. O.; Wallace, G. G. *Chem. Mater.* **2008**, *20*, 2603.

(3) Bruce, P. G.; Scrosati, B.; Tarascon, J.-M. *Angew. Chem., Int. Ed.* **2008**, *47*, 2930.

(4) (a) Wei, G.; Ma, P. X. *Adv. Funct. Mater.* **2008**, *18*, 3568. (b) Guo, Y.; Shi, D.; Cho, H.; Dong, Z.; Kulkarni, A.; Pauletti, G. M.; Wang, W.; Lian, J.; Liu, W.; Ren, L.; Zhang, Q.; Liu, G.; Huth, C.; Wang, L.; Ewing, R. C. *Adv. Funct. Mater.* **2008**, *18*, 2489. (c) Paunesku, T.; Rajh, T.; Wiederrecht, G.; Maser, J.; Vogt, S.; Stojićević, N.; Protić, M.; Lai, B; Oryhon, J.; Thurnauer, M.; Woloschak, G. *Nat. Mater.* **2003**, *2*, 343.

(5) (a) Bronstein, L. M.; Joo, C.; Karlinsey, R.; Ryder, A.; Zwanziger, J. W. *Chem. Mater.* **2001**, *13*, 3678. (b) Liu, J.; Yang, Q.; Zhang, L.; Yang, H.; Gao, J.; Li, C. *Chem. Mater.* **2008**, *20*, 4268. (c) Gao, Q.; Chen, P.; Zhang, Y.; Tang, Y. *Adv. Mater.* **2008**, *20*, 1837.

(6) (a) Hartmann, M. *Chem. Mater.* **2005**, *17*, 4577. (b) Vinu, A.; Murugesan, V.; Tangermann, O.; Hartmann, M. *Chem. Mater.* **2004**, *16*,

3056. (c) Vinu, A.; Murugesan, V.; Hartmann, M. *J. Phys. Chem. B* **2004**, *108*, 7323. (d) Vinu, A; Miyahara, M.; Ariga, K. *J. Phys. Chem. B* **2005**, *109*, 6436.

(7) (a) Zhang, L.; Zhang, Q.; Li, J. *Electrochem. Commun.* **2007**, *9*, 1530. (b) Jia, N.; Wen, Y.; Yang, G.; Lian, Q.; Xu, C.; Shen, H. *Electrochem. Commun.* **2008**, *10*, 774.

(8) (a) Jia, N.; Lian, Q.; Shen, H.; Wang, C.; Li, X.; Yang, Z. *Nano Lett.* **2007**, *7*, 2976. (b) Feazell, R. P.; Nakayama-Ratchford, N.; Dai, H.; Lippard, S. J. *J. Am. Chem. Soc.* **2007**, *129*, 8438.

(9) (a) Zhu, L.; Yang, R.; Zhai, J.; Tian, C. *Biosens. Bioelectron.* **2007**, *23*, 528. (b) Besteman, K.; Lee, J.-O.; Wiertz, F. G. M.; Heering, H. A.; Dekker, C. *Nano Lett.* **2003**, *3*, 727. (c) Lin, Y.; Lu, F.; Tu, Y.; Ren, Z. *Nano Lett.* **2004**, *4*, 192.

(10) (a) Vallet-Regí, M.; Rámila, A.; Del Real, R. P.; Pérez-Pariente, J. *Chem. Mater.* **2001**, *13*, 308. (b) Anderson, J.; Rosenholm, J.; Areva, S.; Lindén, M. *Chem. Mater.* **2004**, *16*, 4160. (c) Slowing, I. I.; Trewyn, B. G.; Lin, V.S.-Y. *J. Am. Chem. Soc.* **2007**, *129*, 8845.

(11) Kost, J.; Langer, R. *Adv. Drug Delivery Rev.* **2001**, *46*, 125.

(12) Santini, J. T., Jr.; Richards, A. C.; Scheidt, R.; Cima, M. J.; Langer, R. *Angew. Chem., Int. Ed.* **2000**, *39*, 2396.

(13) Munoz, B.; Rámila, A.; Pérez-Pariente, J.; Diaz, I.; Vallet-Regí, M. *Chem. Mater.* **2003**, *15*, 500.

(14) Das, S. K.; Kapoor, S.; Yamada, H.; Bhattacharyya, A. J. *Mesoporous Microporous Mater.* **2009**, *118*, 267.

(15) Kovtyukhova, N. I.; Mallouk, T. E.; Mayer, T. S. *Adv. Mater.* **2003**, *15*, 780.

(16) Nishiharaa, H.; Fukuraa, Y.; Indea, K.; Tsuji, K.; Takeuchi, M.; Kyotani, T. *Carbon.* **2008**, *46*, 48.

(17) Heating at 800 °C (for 4 h) resulted in carbonization of DN and subsequent coverage of SNT surface with carbon. The carbonized SNT resulted in very poor IBU loading yields and hence are not discussed here.

(18) Kamegawa, K.; Yoshida, H. *J. Colloid Interface Sci.* **1993**, *159*, 324.

(19) Kokubo, T.; Kushitani, H.; Sakka, S.; Kitsugi, T.; Yamamuro, T. *J. Biomed. Mater. Res.* **1990**, *24*, 721.

(20) Zygmunt, J.; Krumeich, F.; Nesper, R. *Adv. Mater.* **2003**, *15*, 1538.

(21) Socrates G. Infrared characteristic group frequencies New York: John Wiley; 1980.

(22) Jentys, A.; Pham, N. H.; Vinek, H. *J. Chem. Soc., Faraday Trans.* **1996**, *92*, 3287.

(23) Hair M. L. *Infrared spectroscopy in surface chemistry*; Marcel Dekker: New York, 1967.

(24) Son, S. J.; Bai, X.; Nan, A.; Ghandehari, H.; Lee, S. B. *J. Controlled Release* **2006**, *114*, 143.

(25) http://www.fda.gov/Cder/Offices/OPS_IO/MRTD.htm.

(26) Costa, P.; Lobo, J. M. S. *Eur. J. Pharm. Sci.* **2001**, *13*, 123.

(27) Kim, H.-J.; Matsuda, H.; Zhou, H.; Honma, I. *Adv. Mater.* **2006**, *18*, 3083.

(28) Kwon, I. C.; Bae, Y. H.; Kim, S. W. *Nature (London)* **1991**, *354*, 291.

(29) Paddon, C.; Marken, F. *Electrochem. Commun.* **2004**, *6*, 1249.

JP9000863